THE JOURNAL OF PHYSICAL CHEMISTRY C

ARTICLE

pubs.acs.org/JPCC

Phase Transitions of Water in Graphite and Mica Pores

Rajat Srivastava,[†] Hugh Docherty,[‡] Jayant K. Singh,[*,†] and Peter T. Cummings[*,‡,§]

[†]Department of Chemical Engineering, Indian Institute of Technology Kanpur, Kanpur 208016, India

[‡]Department of Chemical and Biomolecular Engineering, Vanderbilt University, Nashville, Tennessee 37235-1604, United States

[§]Center for Nanophase Material Science, Oak Ridge National Laboratory, Oak Ridge, Tennessee 37831-6494, United States

ABSTRACT: We report all-atom molecular dynamics simulations of water confined in graphite and mica slit pores of variable size ranging from 10 to 60 Å. For each pore size, we demonstrate that the confinement not only reduces the critical temperature of the water but also introduces inhomogeneity in the system that, in turn, results in different vapor−liquid coexistence densities at different layers of the pore. We report, in detail, the contribution of different layers toward the vapor−liquid phase diagram of the confined water in graphite and mica slit pores. We also present the hydrogen bonding (HB) distribution in various layers and the ordering of water molecules near the surface of pore. Bond orientational order calculations of water near the surface of the pores indicate that water molecules tend to order near the mica surface whereas the ordering is absent for the case of graphite pores.

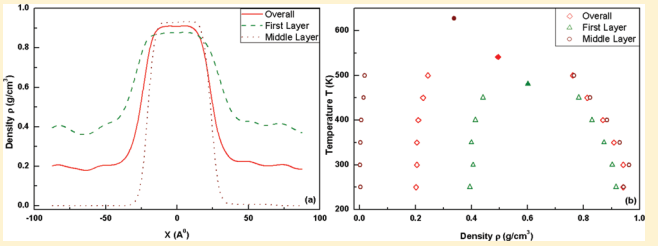

1. INTRODUCTION

Water is the most abundant liquid on Earth's surface. It plays a vital role in living organisms and most terrestrial chemical reactions. In recent years, water in confined environments has attracted considerable attention due to its importance in understanding many biological and geological processes as well as for advancing technological developments at the nanoscale. For example, in living cells, where water is confined in nanoscale cavities of biomolecules, it plays an important role in regulating hydrophobic collapse leading to protein-folding.[1,2] In the field of nanotribology, confined water acts as a lubricant between two surfaces with the friction between the confining surfaces being strongly influenced by the thickness of the confined water film.[3,4] This has important implications for lab-on-a-chip applications,[5] etc. Hence, while understanding the phase behavior, as well as the structural and dynamical properties, of confined water is a complex and daunting task because of the anomalous behavior of water inside confined geometries, it continues to be a subject of increasing interest in recent years.

An extensive review of the computer simulation studies of water under confinement was conducted by Zangi,[6] who also reported that varying the slit width of a quartz-based slitpore leads to sequential freezing and melting of a monolayer and a bilayer water at ambient temperature. Further to this, he also reported that confinement promotes freezing because of a small difference in the free energy of liquid phase and solid phase under confinement compared to bulk fluid due to a reduction in entropy of the system. Koga et al.[7] performed classical molecular dynamics simulations of water confined inside carbon nanotubes (CNTs) of diameter ranging from 1.1 to 1.4 nm, noting the existence of new ice phases which are absent in bulk ice. Meanwhile, Hummer et al.[8] addressed fast diffusion of water inside CNTs using MD simulations resulting from tight hydrogen bonding between water molecules and weak attraction between water and CNT leading to burst-like flow of water with little resistance. Finally, Brovchenko and co-workers[9,10] extensively studied vapor−liquid phase transition of water under hydrophobic and hydrophilic confinement for slit and cylindrical pores showing that, in nanoscale pores, many water properties differ drastically from those of bulk water. They have shown that the critical temperature decreases with decreasing pore width. Further to this, Brovchenko and co-workers[9,11] studied the effect of hydrophobic and hydrophilic groups on biomolecular surfaces on the hydration of water near biosurfaces, which plays a vital role in structure and functioning of biosystems. They also studied[12] the temperature dependence of isobaric specific heat capacity C_p of the hydration water in hydrophobic and hydrophilic peptides and reported that the C_p of water in the hydration shells of both peptides exceeds the bulk value and decreases upon heating. Recently, Giovambattista et al.[13] performed molecular dynamics simulation of water in a hydrophobic slit pore and reported that there is a first-order transition from bilayer liquid (BL) to trilayer heterogeneous fluid (THF) with increasing density of water. They also observed a similar effect with respect to pore width, specifically noting a transformation of THF into bilayer ice with a decrease in pore width.

Despite this wealth of research, a number of key issues remain unsolved. For instance, it is not clear how confining surfaces influence the structural and dynamic behavior of confined water, particularly what is the impact of hydrophobic versus hydrophilic surfaces, since most of the work performed until now has used structureless model surfaces. In fact, even using these more simplistic models, little work has been performed related to the

Received: January 12, 2011
Revised: May 16, 2011
Published: May 23, 2011

phase diagram of confined water. In addition, phase diagram calculations are mainly being reported using overall density in the pore as the order parameter. However, it is well-known that a fluid phase under confinement is usually inhomogeneous.[10] Hence, the question arises: how do different layers under confinement contribute to the overall phase diagram? Some work in this direction has already been addressed by Brovchenko and coworkers[10] where they have analyzed the surface phase transition and nature of the various layers as found in confined fluids in structureless pores. Recently, Mercado et al.[14] performed Monte Carlo simulations to calculate the vapor−liquid equilibria of a square-well (SW) fluid at the surface and center of a cylindrical pore and found that there is a difference in the coexistence densities and, consequently, different phase diagrams. Similarly, Nguyen et al.[15] have studied the adsorption of noble gases and nitrogen on a graphitic surface using Grand Canonical Monte Carlo (GCMC) simulations and characterized the adsorbate in terms of the critical temperature of different adsorbed layers.

Though the above examples show that some efforts have been made to understand the nature of various layers under confinement, such studies have typically made use of simplistic structureless confining surfaces while studies attempting to capture the atomistic nature of these systems are, by comparison, rare. Given that when working at the nanoscale surface effects are known to be crucial, it seems likely that our understanding of such systems is incomplete. Therefore, in the current work, we present the phase transition, using all-atom molecular dynamics simulations, of water confined in graphite and mica slit pores of variable size. We also present, in detail, hydrogen bond distribution in coexisting vapor and liquid phases of the confined water and the contribution of various layers under confinement toward the overall phase diagram of water for various pore sizes. In addition, we also analyze the hexatic orientational order parameter of the liquid phase in first layer of water inside graphite and mica pores.

2. SIMULATION DETAILS

2.1. Potential Model. The TIP4P/2005 model is used for water,[16] interaction parameters for graphite−water (σ_{CO} = 3.262 Å and ε_{CO} = 0.0926 kcal/mol) are those used by Koga et al.,[7] and a fully flexible atomistically detailed model[17,18] (Table 1) of a mica surface consisting of two mica sheets is used to perform the simulations. Each graphite surface consists of two layers of carbon atoms separated by 1.53 Å with an interlayer separation of 3.4 Å. van der Waals interactions between atoms are described by the 12−6 Lennard−Jones (LJ) potential, and the particle−particle particle−mesh (PPPM) technique is applied to account for long-ranged electrostatic forces. The nonbonded interactions are described by Lennard−Jones and Coulomb potential:

$$U_{\text{nonbonded}} = 4\varepsilon_{ij}\left[\left(\frac{\sigma_{ij}}{r}\right)^{12} - \left(\frac{\sigma_{ij}}{r}\right)^{6}\right] + \frac{q_i q_j}{4\pi\varepsilon_0 r_{ij}} \quad (1)$$

where ε_{ij}, σ_{ij}, q_i, and ε_0 are the characteristic energy, size parameters, partial charge, and permittivity of free space, respectively, and r_{ij} is the distance between the centers of mass of the pair of atoms. Bond stretching and bending are described by a harmonic potential

$$U_{\text{stretching}} = \frac{1}{2}k_l(l - l_0)^2 \quad (2)$$

Table 1. Force Field Parameters for the Mica Surface[17]

nonbonded	charge	σ (Å)	ε (kcal/mol)
K	+1.0	3.38542	0.20
$Si^{surface}$	+1.1	3.56359	0.05
$Al^{surface}$	+0.8	3.74178	0.05
$Al^{octahedral}$	+1.45	3.74178	0.05
$O^{surface}$	−0.55	3.11815	0.025
O^{apical}	−0.758	3.11815	0.025
$O^{hydroxyl}$	−0.683	3.11815	0.025
$H^{hydroxyl}$	+0.20	0.978296	0.013
bonds		l_0 (Å)	k_l (kcal/mol·Å^2)
all bonds between Si, O, Al		exptl[18]	860
O−H		0.929	990
angles		θ_0 (deg)	k_θ (kcal/mol·rad^2)
all angles between Si, O, Al		exptl[18]	340
H−O−Al		116.2	23

and

$$U_{\text{bending}} = \frac{1}{2}k_\theta(\theta - \theta_0)^2 \quad (3)$$

where k_1 and k_θ are force constants, l, θ, l_0, and θ_0 are bond length, bond angle, and their corresponding equilibrium values, respectively.

2.2. Simulation Method. Simulations are performed using the LAMMPS[19] molecular dynamics package, and periodic boundary conditions are applied along the unbounded directions x and y. We have considered water confined inside two parallel graphite or mica surfaces. The surfaces, separated by a distance H, are symmetrical about the center of simulation box such that they are parallel to the $x-y$ plane and equidistant (H/2) from the $z = 0$ plane. In this work, the distance between the pore walls, the pore width (H), varies from 10 Å to 60 Å. We set up a simulation box of lengths L_x, L_y, and L_z in the x,y, and z directions, respectively, defined such that x and y are parallel to, and z perpendicular to, the pore wall. To accommodate the formation of vapor and liquid phases, we study the structural properties of confined water using MD simulations in the canonical (constant number of atoms N, constant volume V, and constant temperature T, or NVT) ensemble with the Nosé−Hoover thermostat. Long range interactions are treated using the particle−particle particle−mesh (PPPM) technique. The two-dimensional corrections have been employed in a similar way as used by Gordillo et al.[20] The equilibration time is set to be 0.5 ns with a time step of 0.001 ps, with production times of 0.5 ns.

In the present work, we have estimated the vapor−liquid critical parameter by fitting the coexistence densities to the law of rectilinear diameter[21] and the scaling law for the density.[22]

$$(\rho_l - \rho_v) = B(1 - \frac{T}{T_c})^\beta \quad (4)$$

$$(\frac{\rho_l + \rho_v}{2}) = \rho_c + A(1 - \frac{T}{T_c}) \quad (5)$$

where ρ_l, ρ_v, ρ_c, T_c, and β are the liquid-phase density, vapor-phase density, critical density, critical temperature, and critical exponent, respectively, and A and B are fitting parameters.

Finally, because hydrogen bonding (HB) plays a vital role in determining the structural and dynamical behavior of water,[23] we

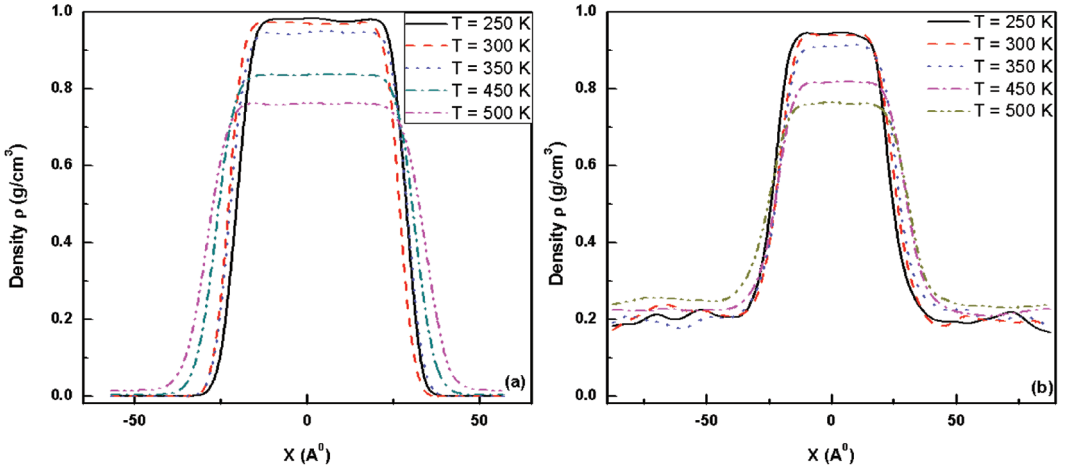

Figure 1. Density profile in the x direction of confined water exhibiting vapor−liquid coexistence inside a graphite pore (a) and mica pore (b) of width $H = 40$ Å.

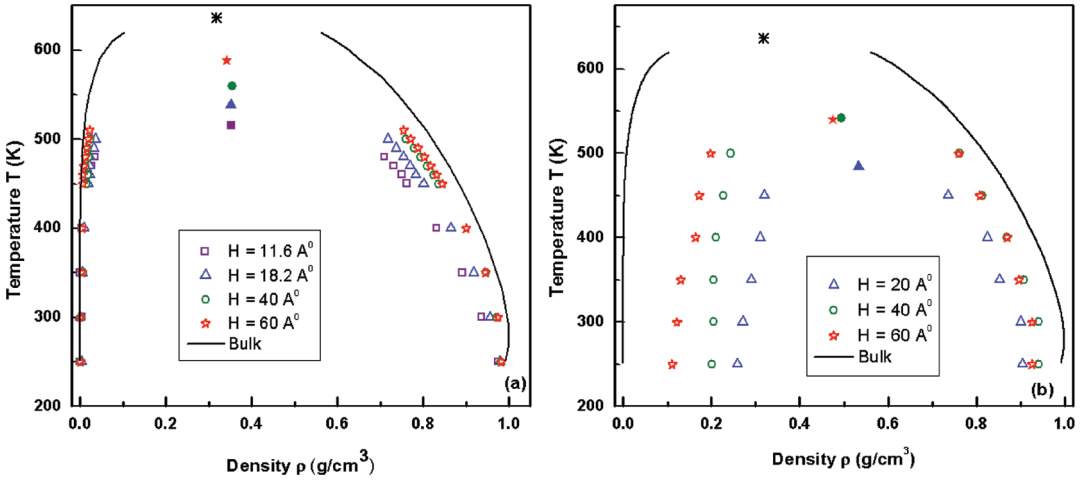

Figure 2. Vapor−liquid coexistence curve of water confined in graphite pore (a) and mica pore (b) with variable slit width. Solid curves represent the bulk coexistence densities with crossed plus symbol as the bulk critical points. Open and filled symbols represent the coexistence densities and critical points, respectively.

investigate the effect of the confining surfaces on the HB distribution of coexisting phases using the geometrical criteria as described by Swiatla-Wojcik.[24]

3. RESULTS AND DISCUSSION

The present work illustrates the effect of confinement and the nature of the confining surface on the vapor−liquid coexistence curve of water. We start with the phase diagram of the confined water. Figure 1, panels a and b, shows the two-phase density profile of water inside graphite and mica pores of pore width $H = 40$ Å, respectively, at different temperatures. The behavior of the density profile is akin to the bulk behavior, i.e., the liquid phase density decreases and the vapor-like density increases with increasing temperature. It can also be seen from the figures that the density of the vapor phase of water is much higher in the case of a mica pore in comparison to a graphite pore. This is attributed to the hydrophilic nature of the mica surface that allows more adsorption on the surface of the pore, leading to ordering of molecules in the vapor phase near the surface of mica at low temperatures.

In Figure 2, panels a and b, we have plotted the vapor−liquid phase diagram of water confined inside graphite and mica slit pores for widths ranging from 10 to 60 Å. For comparison, the vapor−liquid phase diagram of bulk water is also included in the figures. Figure 2, panels and b, reveals that there is a lowering of the critical temperature of water confined inside slit pores in comparison to the bulk case. In addition, in Figure 2a, it is seen that while nanoconfinement between graphite sheets results in a decrease in the liquid phase density as a function of decreasing slit width, its effect on the vapor phase is minimal. Thus, the coexistence curve becomes narrower, leading to a reduction in the critical temperature and a flattening of the vapor−liquid coexistence curve with decreasing pore width because of the shrinking of coexistence curve, while the critical density remains largely unchanged. From Figure 2b, we note that, as in the case of graphite, nanoconfinement between mica sheets results in a decrease in the liquid phase density as a function of decreasing pore width. However, in contrast to the case of graphite sheets, we observe a dramatic increase in the vapor phase density with decreasing pore width, with the result that the critical density shifts to larger values.

dx.doi.org/10.1021/jp2003563 |J. Phys. Chem. C 2011, 115, 12448–12457

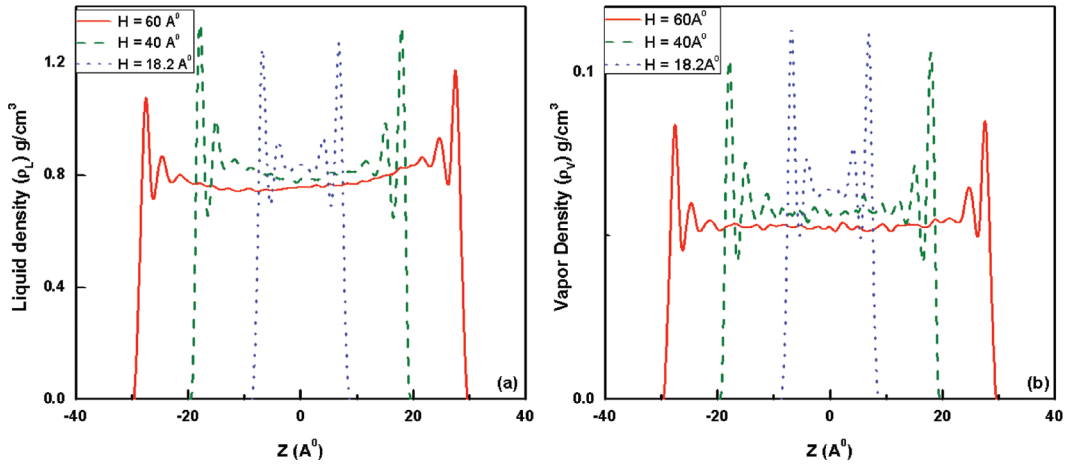

Figure 3. Density profile in the z direction of water in the liquid phase (a) and vapor phase (b) confined inside a graphite slit pore at T = 350 K.

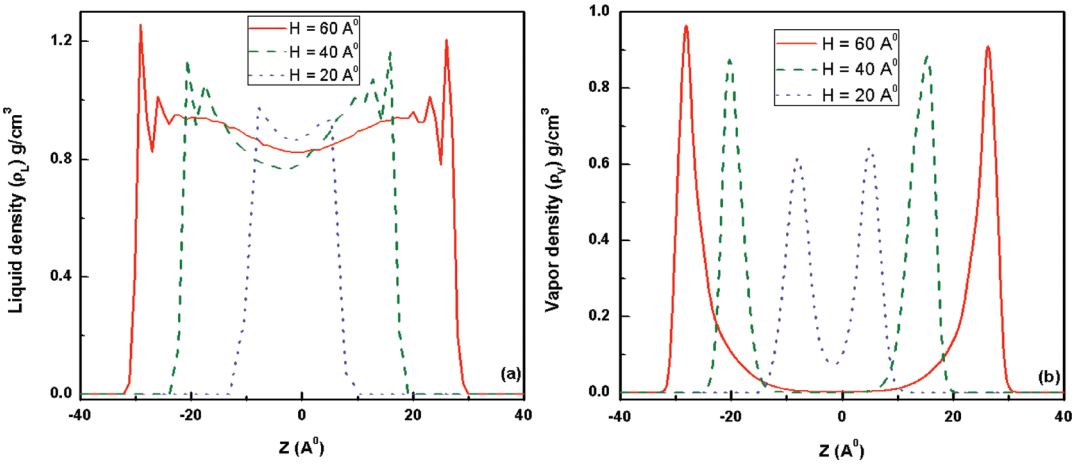

Figure 4. Density profile in the z direction of water in the liquid phase (a) and vapor phase (b) confined inside a mica slit pore at T = 350 K.

Thus, from Figure 2, we can say that the presence of a hydrophilic surface (mica) not only affects the liquid phase density (as in the case of graphite pores) but also affects the vapor phase density, which in turn leads to the reduction of the critical temperature because of a narrowing of the vapor−liquid coexistence curve. Similar evidence of a lowering of critical temperature has been reported by Mercado et al.[14] and Singh et al.[25] for square well fluid under confining surface. Figure 2, panels a and b, also suggests that the pore critical temperature of water inside a mica pore is lower than that of a graphite pore, from which we conclude that an increase in hydrophilicity decreases the critical temperature. Additionally, it is worth noting that, in the case of the mica pore (Figure 2b), an increase in the critical density is observed with decreasing slit width because of the considerable shift in the vapor phase density.

From Figure 2, panels a and b, it is clear that the presence of confining surfaces affect the critical properties of water; however, they also affect the wider range of thermodynamic conditions. For example, it has been reported that, in the presence of confining surfaces, fluid becomes inhomogeneous.[10] Evidence of this may be seen in the density profile of the liquid and vapor phases of water perpendicular to the confining surfaces. Such profiles, for graphite and mica pores, are shown in Figures 3 and 4, respectively. Starting with Figure 3a, corresponding to the liquid phase of water between graphite sheets at 350 K, we note the presence of multiple peaks (in case of H = 60 Å and 40 Å) near the surface and a constant density region at the center of pore, which disappears with reduction in pore width. A similar pattern is observed in the case of the vapor phase density profile (shown in Figure 3b). Moving to the case of mica slit pores (Figure 4, panels a and b), we note that, in common with graphite sheets, the liquid phase shows two peaks near the surface for larger separations. However, for the smaller gap height of 20 Å, this second peak disappears. While similarities may be seen in the liquid phase behaviors, the vapor phase density profile of water nanoconfined in a mica slit pore exhibits totally different behavior when compared to a graphite pore. Specifically, near the surface, the vapor phase density is much higher than that in a graphite pore and consists of only a single peak.

From Figures 3 and 4, it is clear that when water is nanoconfined, there is a layering of water molecules near the surface, resulting in a heterogeneous water density in the slit pore. This, in turn, results in different regions of the pore having different thermodynamical properties. This can be regarded as an extension of analyses that focus on the phase behavior in the adsorbed monolayer on the surface.[15] Clearly, from an experimental point of view, the critical properties observed are an average over the pore. However, part of what makes molecular simulation such a powerful tool is that it allows us to probe the properties of

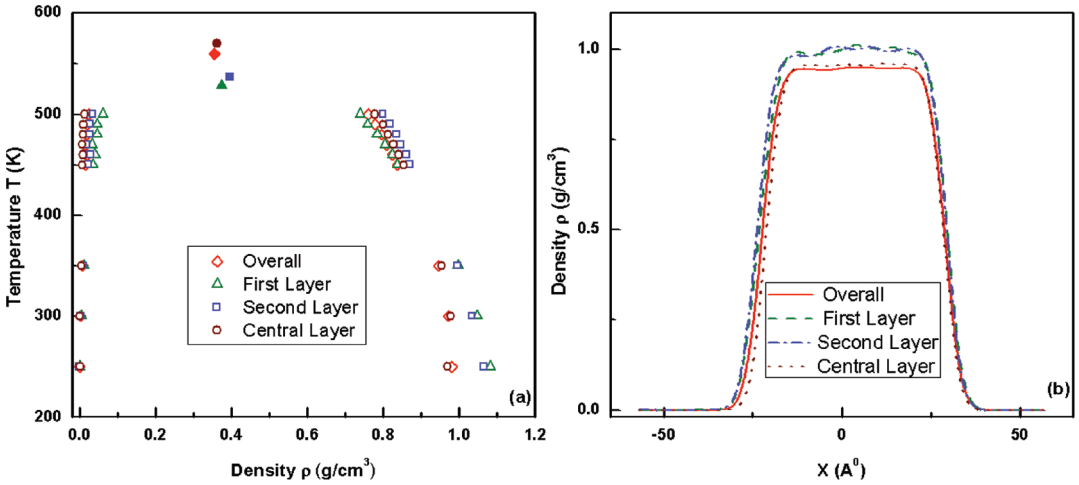

Figure 5. (a) Vapor−liquid coexistence curves at H = 40 Å for the different layers of water confined under a graphite slit pore. Open and filled symbols represent the coexistence densities and critical points, respectively. (b) Density profiles in the x direction for the different layers of water confined inside a graphite slit pore at T = 350 K and H = 40 Å.

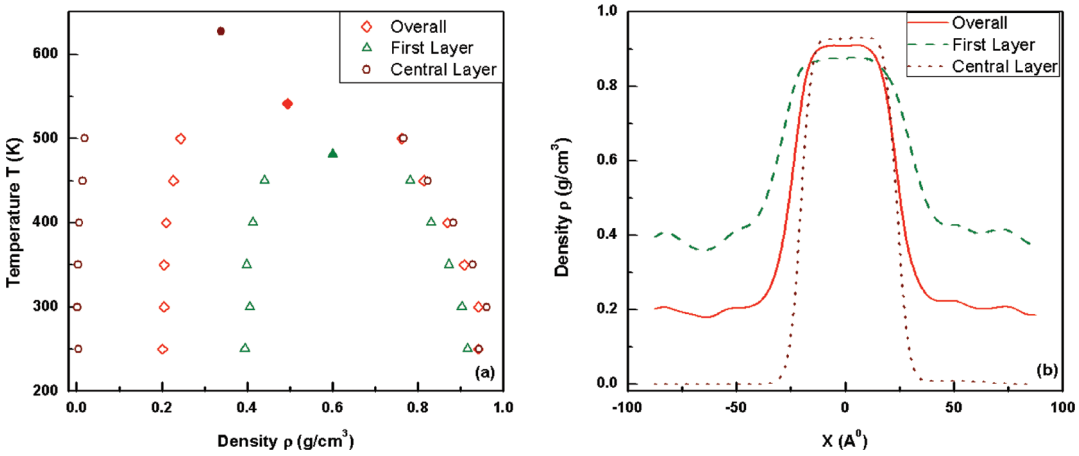

Figure 6. (a) Vapor−liquid coexistence curves at H = 40 Å for the different layers of water confined under mica slit pore. Open and filled symbols represent the coexistence densities and critical points respectively. (b) Density profile in the x direction for the different layers of water confined inside mica slit pore at T = 350 K and H = 40 Å.

systems in ways that, while possibly artificial in nature, provide valuable insight into the factors determining the overall behavior of a system. With regards to the systems studied here, it is possible to improve our understanding of what occurs in nanoconfined fluids by dividing the confined fluid into layers and considering the phase equilibria in a layer-by-layer manner. Hence, one of the objectives of this work is to understand the phase diagram of different layers and their effective contribution to the overall pore phase diagram.

Specifically, we investigate the critical properties of the first layer (surface layer), second layer, and central layer (center of the pore) of water in the pore. Results for a 40 Å graphite slit pore are presented in Figure 5a and clearly illustrate that, relative to the other layers, the first layer experiences a greater reduction in liquid saturation density and a larger increment in vapor saturation density with increasing temperature. Hence, a reduction of the critical temperature has been observed for the first layer. On the other hand, in the central layer the liquid density and vapor density of water approaches the bulk value, which results in a critical temperature higher than that obtained for the first layer. The critical temperature of the second layer is found to be between that of the central and first layers, although its liquid density is higher than the central layer due to a larger vapor density. The above is also evident from the x-direction density profile (Figure 5b). Interestingly, the results presented here for water in a graphitic pore suggest behavior similar to that of noble gases on graphite surfaces as recently demonstrated by Nguyen et al.[15] using molecular simulation. Specifically, they note that the critical temperature of the surface layer is lower compared to that of the higher layers.

In the case of the mica slit pore, layering near the surface is observed; however, we do not observe multiple layering in the vapor phase (see Figure 4b). Hence, we calculate only the critical properties of water in the first layer (surface layer) and central layer in mica pores. Because mica is hydrophilic in nature, it adsorbs more water molecules and wets the surface; as a result, its vapor density near the surface is dramatically higher than the center of the pore (Figure 4b). At the same time, a corresponding reduction in liquid density near the pore wall results in a contraction of the VLE curve, leading to a reduction in critical temperature (Figure 6a). In the central layer the liquid phase density is higher and the vapor

dx.doi.org/10.1021/jp2003563 |J. Phys. Chem. C 2011, 115, 12448–12457

phase density is lower than that of the surface layer; hence, its critical temperature is much higher. The above is also evident from the x-direction density profile as shown in Figure 6b. An increase in the critical density of the water inside the first layer, with respect to the central layer, is also observed in the case of the mica pore. To validate the concept of a first layer critical point, we confirm that the first layer does indeed not exhibit any inhomogeneity beyond our estimated critical point. This is accomplished by performing a simulation at a temperature of T = 530 K, which is slightly higher than the first layer critical temperature. The vapor and liquid density profiles from this simulation are shown in Figure 7 and clearly illustrate that only the central layer is under a two-phase region. This suggests strongly that the contribution to the overall phase diagram may vary as a function of temperature, with the first layer not contributing beyond a certain temperature. As shown in Figure 8, similar evidence is also observed for narrower mica and graphite pores.

We move now to the shape of the vapor−liquid coexistence curve, which can be determined by using the relationship between the order parameter $(\Delta\rho)$ and the reduced temperature deviation $\tau = (T_c^{bulk} - T)/T_c^{bulk}$, where T_c^{bulk} is the bulk critical temperature of TIP4P water. With increasing temperature, the coexisting liquid and vapor phase densities approach each other, and below the critical temperature the difference between liquid densities (ρ_l) and vapor densities (ρ_v) obeys the universal scaling law[26,27]

$$\Delta\rho = \left(\frac{\rho_l - \rho_v}{2}\right) \sim \tau^{\beta} \qquad (6)$$

where β is critical exponent of the order parameter. As reported earlier, in the presence of a surface, a fluid become inhomogeneous and all the properties of the fluid become local. Hence, we have calculated a local order parameter for each of the different layers of confined water. Figure 9, panels a and b, reports the order parameter $(\Delta\rho)$ as a function of reduced temperature (τ) in log−log scale for water inside a graphite and mica slit pore, respectively. The slope of the curve is represented by β for different layers of water confined in a slit pore. In the case of graphite, the value of β for the first, second, and central layers are 0.63, 0.3393, and 0.3210, respectively. In the case of the mica slit pore, an exponent value (β) of 0.7612 and 0.2908 is found for the first and central layers of the confined water, respectively. By comparing these values to the surface critical exponent of ordinary transition[28] $(\beta \approx 0.82)$ in Ising magnets, in the absence of a surface field and the bulk Ising value, i.e. $(\beta \approx 0.326)$, it is clear that while the behavior of β for the second and central layers are similar to the bulk, the first layer behaves in a manner consistent with quasi-2D localization of the water molecules near the surface of the pore. Additionally, we note that this is more pronounced in the case of hydrophilic pores.

Of course, no investigation involving water would be complete without a discussion of hydrogen bonding, so we now consider the effect of confinement on the hydrogen bonding of water. To date, a number of works have shown that confinement can result in a substantial decrease in hydrogen bonding. For example, an 88% reduction in HB is observed by Han et al.[29] for water confined in hydrophobic pores, consistently over a range of temperatures, and Debenedetti and co-workers[30] have reported the average HB as a function of distance from the surface. However, until now, the differences, if any, between the hydrogen bonding of water molecules in various layers of coexisting phases of confined water has remained unclear. To clarify this issue, we have calculated the average HB distribution of water by layer for both the graphitic and mica pore considered in this work at a temperature of 350 K.

We start by considering the overall average HB distributions for the liquid (Figure 10a) and vapor (Figure 10b) phases. We

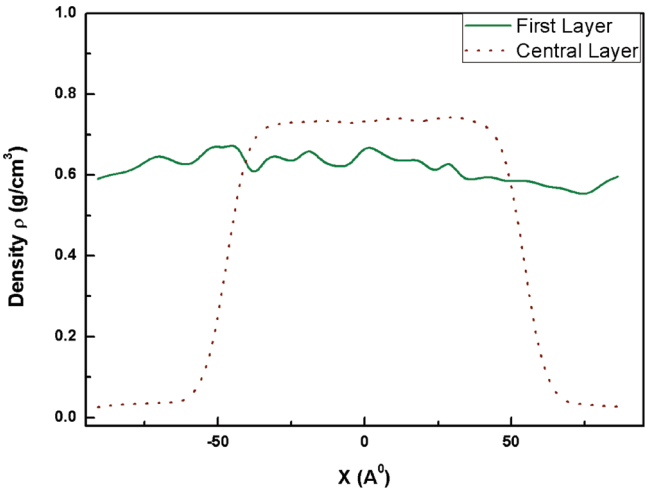

Figure 7. Density profile in the x direction of the first and central layer of confined water inside a mica pore of width H = 40 Å at T = 530 K.

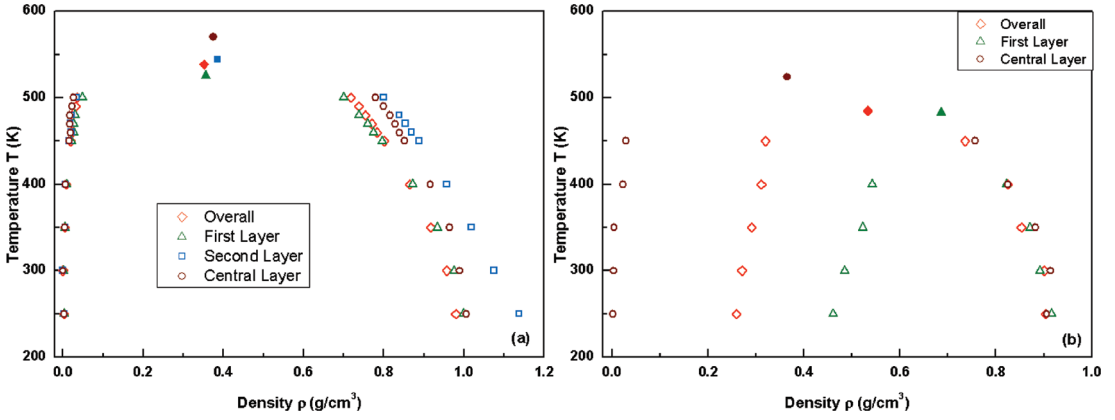

Figure 8. Vapor−liquid coexistence curve of different layers of water confined under a graphite slit pore (H = 18.2 Å) (a) and mica slit pore (H = 20 Å) (b). Open and filled symbols represent the coexistence densities and critical points, respectively.

dx.doi.org/10.1021/jp2003563 |J. Phys. Chem. C 2011, 115, 12448–12457

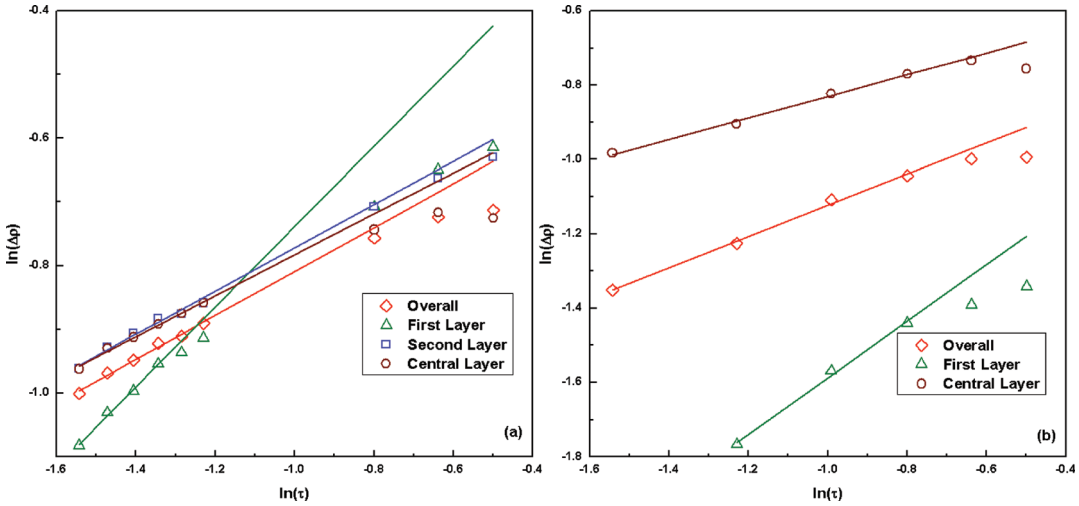

Figure 9. Log−log plot of order parameter ($\Delta\rho$) with reduced temperature (τ) for water confined in 40 Å of a graphite pore (a) and mica pore (b).

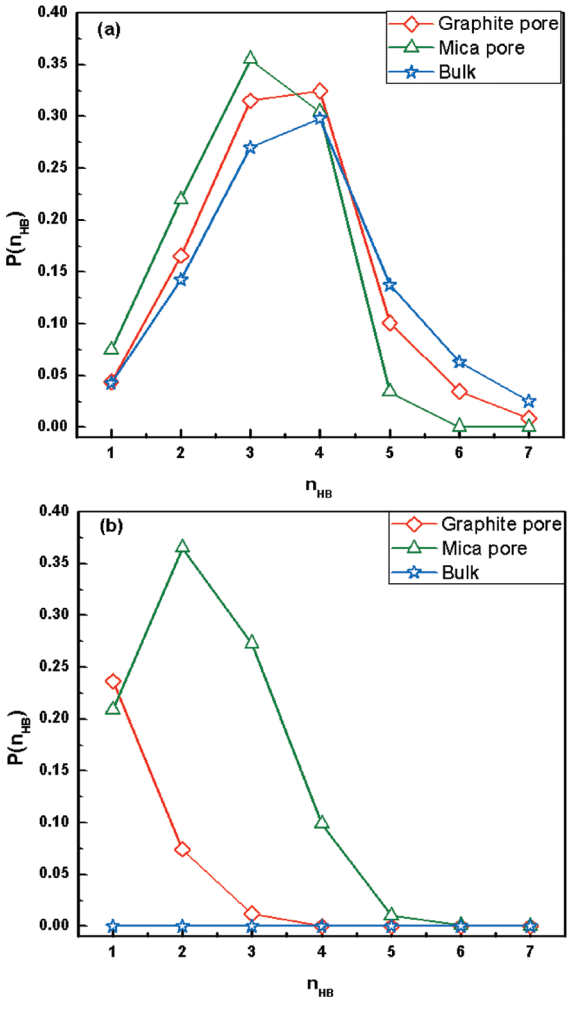

Figure 10. Normalized distribution of the number of hydrogen bonds (n_{HB}) of water confined in 40 Å of a graphite pore and mica pore in liquid phase (a) and vapor phase (b) at T = 350 K. Solid curve with open star symbol represents the distribution of n_{HB} of bulk water.

note that hydrogen bonding in the hydrophobic pore is not fundamentally different than that observed in bulk liquid water, i.e., it shows a maximum probability of n_{HB} = 4 with a significance presence of higher coordination numbers (n_{HB} > 4). However, the occurrence of larger clusters is somewhat suppressed while smaller clusters are enhanced. By contrast, the hydrophilic pore displays a highest probability for n_{HB} = 3 with a bias toward smaller clusters. In fact, larger than n_{HB} = 5 is missing or negligible in the mica pore. Moving to the vapor phase, there is a very obvious and dramatic difference between the confined and bulk water systems. Specifically, while negligible hydrogen bonding occurs in the vapor phase of bulk water, HB is enhanced to such a degree under nanoconfinement that both the hydrophobic and hydrophilic systems considered here exhibit significant hydrogen bonding in the vapor phase. Further, while both confined systems see an increase in hydrogen bonding in the vapor phase, the distribution of the number of bonds differs substantially and the increase in HB is more dramatic in the case of the hydrophilic pore, with the mica pore showing a higher level of hydrogen bonding with a maximum probability of n_{HB} = 2, in contrast to the graphite pore which peaks at n_{HB} = 1 with smooth decrease in the probability distribution for n_{HB} > 1.

With regard to the contributions of the various layers within the system, Figure 11 describes the distribution of HB for each of the layers for the graphite pore. Confined saturated liquid water in hydrophilic pores do not have much different distribution among the layers except the magnitude, as shown in Figure 12. The first layer tends to enhance smaller (and suppresses larger) clusters (coordination number) compared to that in the overall or in the center of pore. On the other hand, different layers in the confined vapor phase in the mica pore are similar to each other, except that the first layer consists of a relatively larger n_{HB} compared to that of the central layer. HB distribution also suggests that central layer in hydrophobic pore is closer to the bulk behavior compared to hydrophilic pore.

Finally, we considered the issue of confinement-induced freezing (i.e., a fluid−solid transition induced by nanoconfinement). There are several studies[31−33] on different fluids which provide evidence of a fluid−solid transition under nanoconfinement. For example, Klein et al.[34] reported a first-order liquid to solid phase transition of OMCTS confined under the mica surface while Radhakrishnan et al.[35] also provided experimental evidence of confinement-induced freezing in the form of differential scanning calorimetry measurements. In addition, Coasne et al.[36] studied argon confined

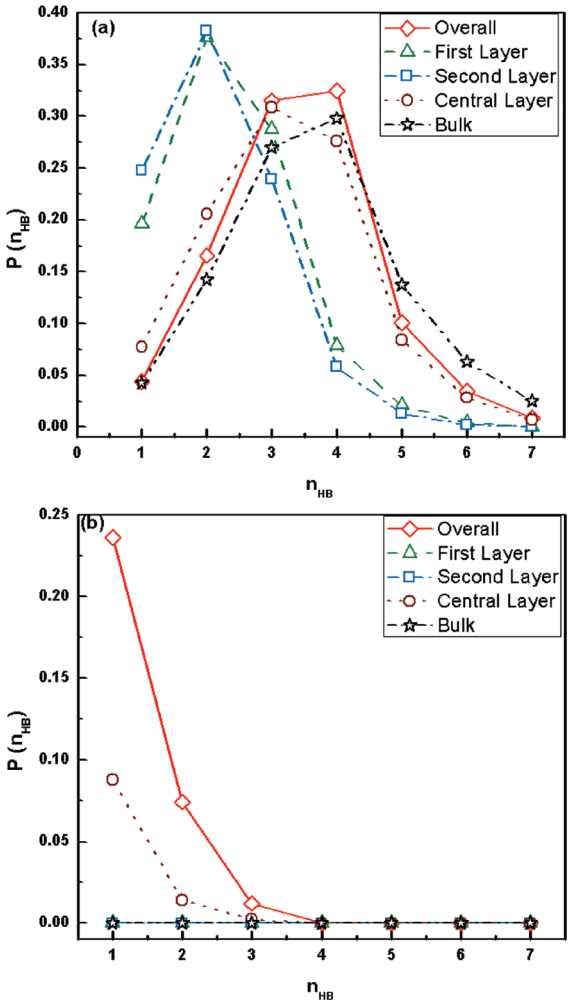

Figure 11. Normalized distribution of number of hydrogen bond in different layers of water in the liquid phase (a) and vapor phase (b) confined inside a graphite pore of width H = 40 Å at T = 350 K.

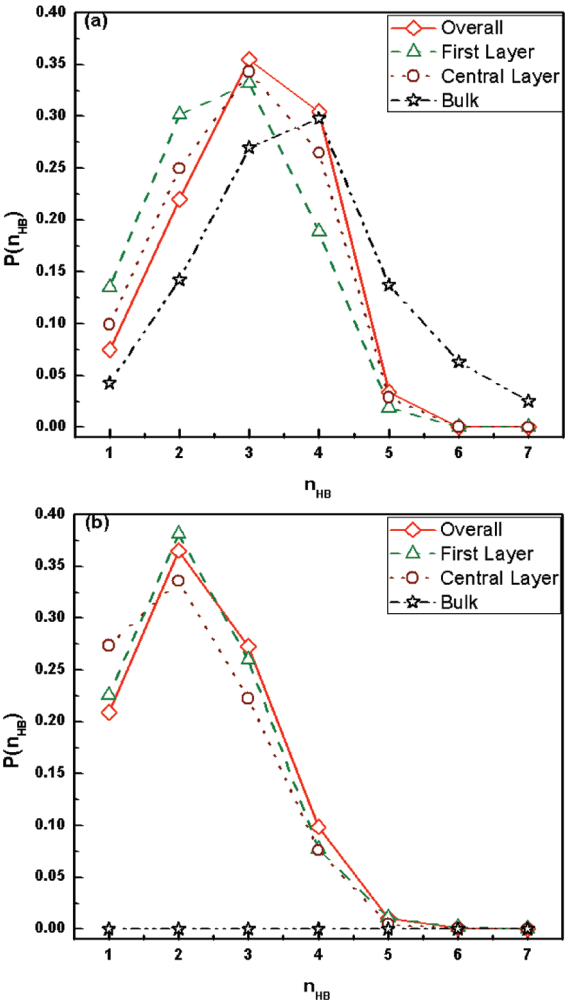

Figure 12. Normalized distribution of the number of hydrogen bonds in different layers of water in the liquid phase (a) and vapor phase (b) confined inside a mica pore of width H = 40 Å at T = 350 K.

under ordered and disordered carbon pores and reported that, in an ordered carbon pore, argon undergoes a phase transition from a 2D liquid state to a hexagonal crystal state that is not observed in the case of a disordered pore. Recently, our group[37,38] also reported that the confining surface plays an important role in the ordering of nonpolar nanoconfined fluids. One of the goals of the present work is to understand the influence of hydrophobic and hydrophilic surfaces on the ordering of molecules near the surface of nanopores.

With this aim in mind, Figures 13 and 14 show snapshots of the first liquid layer of water inside graphite and mica, respectively, and, it would seem, the ordering in the water near the mica surface is not greater than that near the graphite surface. In order to clarify this, we have calculated the in-plane hexatic order parameter[39,40] defined as

$$\psi_6 = \frac{1}{N_b}\sum_{k=1}^{N_b} \exp(i6\theta_k) = \langle \exp(i6\theta_k) \rangle \qquad (7)$$

where ψ_6 measures the in-plane hexagonal bond order. Each nearest neighbor bond has a particular orientation in the plane, with respect to a reference axis, and is described by the polar coordinate θ. The index k spans the total number of nearest neighbor bonds, N_b, in the layer. ψ_6 is close to 1 for a crystalline

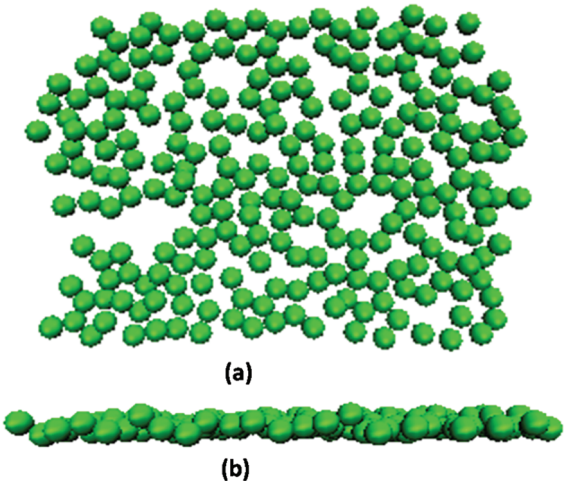

Figure 13. Snapshot of the first layer of oxygen atoms inside a graphite slit pore of width H = 40 Å at T = 350 K: (a) top view; (b) side view.

phase and close to 0 for a liquid phase. In the case of the first liquid layer inside the graphite slit pore, it is close to 0 and for the case of

dx.doi.org/10.1021/jp2003563 |J. Phys. Chem. C 2011, 115, 12448–12457

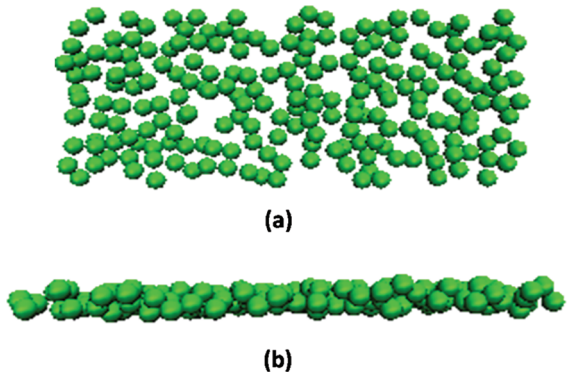

Figure 14. Snapshot of the first layer of oxygen atoms inside a mica slit pore of width H = 40 Å at T = 350 K: (a) top view; (b) side view.

the mica slit pore it is 0.19. This signifies that the first liquid layer in a graphite slit pore is more like a two-dimensional liquid while, by comparison, the first liquid layer in the case of mica is orientationally ordered to a limited degree in a hexatic phase.

4. CONCLUSIONS

We have investigated the influence of hydrophobic and hydrophilic surfaces on the vapor−liquid phase transition of nanoconfined water. Our findings reveal that the presence of hydrophilic (mica) surfaces causes a greater reduction in critical temperature and shift in critical density of confined water in comparison to hydrophobic (graphite) surfaces. This is mainly due to the hydrophilic nature of the mica surface which allows water to wet the surface, leading to considerable increase in vapor phase density compared to the bulk value. We observe an inhomogeniety in the density of coexisting phases of confined water in different regions of the pore. Our results confirm that the vapor−liquid phase behavior is different at the surface and center of the pore. Specifically, molecules in the layers near the surface of a pore behave more like a quasi-2D fluid while layers at the center of a pore behave like bulk water. HB distribution calculations further suggest that the central layer of water in a graphite pore is more bulk-like compared to that in a mica pore. In addition to this, confinement is seen to induce substantial HB in the vapor phase where, by contrast, none is observed for a bulk water system. This is particularly marked for hydrophilic pores. On the other hand, average HB decreases for coexisting confined liquid phases. With regard to critical temperature, for both hydrophilic and hydrophobic pores, this is found to be highest for the central layer and lowest for the surface adjacent layer (first layer). In contrast to this, the critical density of the first layer is highest and that of the central layer is lowest. We also report that the presence of mica (hydrophilic) surfaces leads to an increase in ordering of water molecules near the pore surface in comparison to that seen in graphite (hydrophobic) pores, where the ordering of water is absent.

AUTHOR INFORMATION

Corresponding Author

*E-mail: jayantks@iitk.ac.in (J.K.S.); peter.cummings@vanderbilt.edu (P.T.C.).

ACKNOWLEDGMENT

The research of R.S. and J.K.S. was supported by the Department of Science and Technology, Govt. of India. (grant no. SR/S3/CE/061/2009). H.D. was supported by the U.S. National Science Foundation through grant CHE-0626259. P.T.C.'s contribution to this research was supported as part of the Fluid Interface Reactions, Structure and Transport Center, an Energy Frontier Research Center funded by the U.S. Department of Energy, Office of Science, Office of Basic Energy Sciences under award no. ERKCC61.

REFERENCES

(1) Zhou, R. H.; Huang, X. H.; Margulis, C. J.; Berne, B. J. *Science* **2004**, *305*, 1605.
(2) Hua, L.; Huang, X. H.; Liu, P.; Zhou, R. H.; Berne, B. J. *J. Phys. Chem. B* **2007**, *111*, 9069.
(3) Zhu, Y.; Granick, S. *Phys. Rev. Lett.* **2001**, *87*, 096104.
(4) Raviv, U.; Giasson, S.; Frey, J.; Klein, J. *J. Phys.: Condens. Matter* **2002**, *14*, 9275.
(5) Darhuber, A.; Troian, S. M. *Annu. Rev. Fluid Mech.* **2005**, *37*, 425.
(6) Zangi, R. *J. Phys.: Condens. Matter* **2004**, *16*, S5371.
(7) Koga, K.; Gao, G. T.; Tanaka, H.; Zeng, X. C. *Nature* **2001**, *412*, 802.
(8) Hummer, G.; Rasaiah, J. C.; Noworyta, J. P. *Nature* **2001**, *414*, 188.
(9) Brovchenko, I.; Oleinikova, A. *Interfacial and Confined Water*, 1st ed.; Elsevier: Amsterdam, 2008.
(10) Brovchenko, I.; Geiger, A.; Oleinikova, A. *J. Phys.: Condens. Matter* **2004**, *16*, S5345.
(11) Oleinikova, A.; Brovchenko, I. *Mol. Phys.* **2006**, *104*, 3841.
(12) Oleinikova, A.; Brovchenko, I.; Singh, G. *Eur. Phys. Lett.* **2010**, *90*, 36001.
(13) Giovambattista, N.; Rossky, P. J.; Debenedetti, P. G. *Phys. Rev. Lett.* **2009**, *102*, 050603.
(14) Mercado, Y. R.; Orea, P.; Ramírez, S. L.; Duda, Y. *Phys. A (Amsterdam, Neth.)* **2009**, *388*, 799.
(15) Nguyen, V. T.; Do, D. D.; Nicholson, D. *J. Phys. Chem. C* **2010**, *114*, 22171.
(16) Abascala, J. L. F.; Vega, C. *J. Chem. Phys.* **2005**, *123*, 234505.
(17) Heinz, H.; Koerner, H.; Anderson, K. L.; Vaia, R. A.; Farmer, B. L. *Chem. Mater.* **2005**, *17*, 5658.
(18) Rothbauer, R. *Neues Jahrb. Mineral., Monatsh* **1971**, 143.
(19) Plimpton, S. *J. Comput. Phys.* **1995**, *117*, 1.
(20) Gordillo, M. C.; Nagy, G.; Marti, J. *J. Chem. Phys.* **2005**, *123*, 054707.
(21) Rowlinson, J. S.; Swinton, F. L. *Liquids and Liquid Mixtures*, 3rd ed.; Butterworth: London, 1982.
(22) Rowlinson, J. S.; Widom, B. *Molecular Theory of Capillarity*; Clarendon: Oxford, U.K., 1982.
(23) Luzar, A.; Chandler, D. *Nature* **1996**, *379*, 55.
(24) Swiatla-Wojcik, D. *Chem. Phys.* **2007**, *342*, 260.
(25) Singh, J. K.; Kwak, S. K. *J. Chem. Phys.* **2007**, *126*, 024702.
(26) Binder, K.; Hohenberg, P. C. *Phys. Rev. B* **1974**, *9*, 2194.
(27) Binder, K.; Hohenberg, P. C. *Phys. Rev. B* **1972**, *6*, 3461.
(28) Binder, K. Critical behaviour at surfaces. In *Phase Transitions and Critical Phenomena*; Domb, C., Lebowitz, J. L., Eds.; Academic Press: London, 1983; p 1.
(29) Han, S.; Kumar, P.; Stanley, H. E. *Phys. Rev. E* **2009**, *79*, 041202.
(30) Castrillon, S. R.-V.; Giovambattista, N.; Aksay, I. A.; Debenedetti, P. G. *J. Phys. Chem. B* **2009**, *113*, 1438.
(31) Klein, J.; Kumacheva, E. *J. Chem. Phys.* **1998**, *108*, 6996.
(32) Radhakrishnan, R.; Gubbins, K. E.; Bartkowiak, M. S. *J. Chem. Phys.* **2002**, *116*, 1147.
(33) Cui, S. T.; Cummings, P. T.; Cochran, H. D. *J. Chem. Phys.* **2001**, *114*, 7189.
(34) Klein, J.; Kumacheva, E. *Science* **1995**, *269*, 816.
(35) Radhakrishnan, R.; Gubbins, K. E. *J. Chem. Phys.* **2000**, *112*, 11048.

(36) Coasne, B.; Jain, S. K.; Naamar, L.; Gubbins, K. E. *Phys. Rev. B* **2007**, *76*, 085416.
(37) Docherty, H.; Cummings, P. T. *Soft Matter* **2010**, *6*, 1640.
(38) Cummings, P. T.; Docherty, H.; Iacovella, C. R.; Singh, J. K. *AIChE J.* **2010**, *56*, 842.
(39) Mermin, N. *Phys. Rev.* **1968**, *176*, 250.
(40) Bartkowiak, M. S.; Dudziak, G.; Sikorski, R.; Gras, R.; Radhakrishnan, R.; Gubbins, K. E. *J. Chem. Phys.* **2001**, *114*, 950.